frontiers in Cell and Developmental Biology

ORIGINAL RESEARCH
published: 17 January 2020
doi: 10.3389/fcell.2019.00366

Quantitative Intracellular pH Determinations in Single Live Mammalian Spermatozoa Using the Ratiometric Dye SNARF-5F

*Julio C. Chávez, Alberto Darszon, Claudia L. Treviño and Takuya Nishigaki**

Departamento de Genética del Desarrollo y Fisiología Molecular, Instituto de Biotecnología, Universidad Nacional Autónoma de México, Cuernavaca, Mexico

Intracellular pH (pH_i) plays a crucial role in mammalian sperm physiology. However, it is a challenging task to acquire quantitative single sperm pH_i images due to their small size and beating flagella. In this study, we established a robust pH_i imaging system using the dual-emission ratiometric pH indicator, SNARF-5F. Simultaneous good signal/noise ratio fluorescence signals were obtained exciting with a green high-power LED (532 nm) and acquiring with an EM-CCD camera through an image splitter with two band-pass filters (550–600 nm, channel 1; 630–650 nm, channel 2). After *in vivo* calibration, we established an imaging system that allows determination of absolute pH_i values in spermatozoa, minimizing cell movement artifacts. Using this system, we determined that bicarbonate increases non-capacitated human pH_i with slower kinetics than in mouse spermatozoa. This difference suggests that distinct ionic transporters might be involved in the bicarbonate influx into human and mouse spermatozoa. Alternatively, pH_i regulation downstream bicarbonate influx into spermatozoa could be different between the two species.

Keywords: intracellular pH, alkalization, spermatozoa, dual emission, image splitter, ratiometric

OPEN ACCESS

Edited by:
Tomer Avidor-Reiss, The University of Toledo, United States

Reviewed by:
Shaomin Shuang, Shanxi University, China
Lin Yuan, Hunan University, China

***Correspondence:**
Takuya Nishigaki
takuya@ibt.unam.mx

Specialty section:
This article was submitted to Cell Growth and Division, a section of the journal Frontiers in Cell and Developmental Biology

Received: *13 August 2019*
Accepted: *13 December 2019*
Published: *17 January 2020*

Citation:
Chávez JC, Darszon A, Treviño CL and Nishigaki T (2020) Quantitative Intracellular pH Determinations in Single Live Mammalian Spermatozoa Using the Ratiometric Dye SNARF-5F. Front. Cell Dev. Biol. 7:366. doi: 10.3389/fcell.2019.00366

INTRODUCTION

The pH is fundamental for most proteins to ensure their proper function, as it influences the electrostatic status of their side chains that, in turn, affect protein structure (folding and conformation) and their interaction with other molecules (Zhou and Pang, 2018). Therefore, intracellular pH (pH_i) changes serve as crucial signals in many cell types.

In spermatozoa, pH_i critically regulates motility (Ho et al., 2002; Nishigaki et al., 2014). In mammals, spermatozoa remain quiescent in the epididymis due to the acidic environment created by vacuolar-type H^+-ATPase (V-ATPase) found in the apical plasma membrane of epithelial cells (Acott and Carr, 1984; Brown et al., 1997). Flagellar beating is suppressed in acidic environments as dynein ATPases, the motor molecules that propel the flagellum, are highly pH_i dependent (Crhisten et al., 1983). Upon ejaculation and contact with the seminal fluid sperm pH_i increases, and the flagellum starts beating. The initial flagellar beat is symmetric with low amplitude and high frequency. Subsequently in the oviduct, the flagellar beat pattern becomes vigorous (asymmetric with high amplitude and low frequency), a process called hyperactivation (Ho and Suarez, 2001). Hyperactivated motility is essential for mammalian spermatozoa since it is required to approach the oocyte and to penetrate its investments (Stauss et al., 1995; Suarez and Pacey, 2006). In order to induce and maintain hyperactivation, an increase in intracellular Ca^{2+} concentration ($[Ca^{2+}]_i$)

is required (Ho et al., 2002), which is mediated through a sperm-specific Ca^{2+} channel, named CatSper (Ren et al., 2001). Although there are species-specific activation mechanisms of CatSper (Lishko et al., 2011), this channel is moderately voltage dependent and highly up regulated by intracellular alkalization (Kirichok et al., 2006). In mouse, the sperm-specific Na^+/H^+ exchanger (sNHE) is essential for the regulation of sperm motility and has been proposed as an activator of CatSper by elevating pH_i (Wang et al., 2003; Navarro et al., 2008). On the other hand, in human spermatozoa, a voltage-gated H^+ channel (Hv1) has been documented to be the main H^+ transporter that activates CatSper rather than sNHE (Lishko et al., 2010). In sea urchin sperm, CatSper is a predominant player in chemotaxis toward sperm-attracting peptides (Seifert et al., 2015; Espinal-Enríquez et al., 2017) and sNHE has been shown to be critical for modulating CatSper activity (González-Cota et al., 2015; Windler et al., 2018).

External bicarbonate (HCO_3^-) is fundamental for capacitation in mammalian spermatozoa (Lee and Storey, 1986; Visconti et al., 1995). Both the pH and the HCO_3^- concentration of the oviductal fluid are higher in uterine and tubal fluids compared to plasma (Vishwakarma, 1962). Moreover, pH in the rhesus monkey female tract elevates dramatically, concomitantly with ovulation (Maas et al., 1977), which might promote sperm capacitation *in vivo*. In mammalian spermatozoa, several HCO_3^- transporters were reported as candidates to mediate HCO_3^- influx across the plasma membrane such as Na^+/HCO_3^- cotransporter (NBC) (Demarco et al., 2003), Cl^-/HCO_3^- exchangers (Chavez et al., 2012), and CFTR (Hernández-González et al., 2007; Xu et al., 2007), as well as its indirect entrance via CO_2 diffusion with subsequent hydration by intracellular carbonic anhydrases (CA) (Wandernoth et al., 2010; José et al., 2015). Besides an increase in the pH_i, a cytosolic HCO_3^- elevation is crucial for activation of the sperm soluble adenylyl cyclase (Okamura et al., 1985; Buck et al., 1999).

To understand how sperm pH_i is regulated, it is indispensable to determine where and when it changes in individual cells. Although sperm pH_i measurements in suspension have been performed using fluorescence indicators for more than three decades (Schackmann and Boon Chock, 1986; Darszon et al., 2004; Hamzeh et al., 2019), there are few reports of imaging single sperm pH_i (Zeng et al., 1996; Chávez et al., 2014, 2018; González-Cota et al., 2015). All these experiments were performed with BCECF (Rink et al., 1982), the most popular fluorescent pH_i indicator in cell physiology. This fluorescence probe is ratiometric but requires dual-excitation (Rink et al., 1982). Consequently, there is a time lag between two subsequent images excited by two different wavelengths and therefore, cell movement artifacts can be significant. Furthermore, BCECF is highly phototoxic to cells (Nishigaki et al., 2006), which was also confirmed in this study.

To overcome the BCECF disadvantages stated above we employed SNARF-5F acetoxymethyl ester (AM) (Liu et al., 2001) whose fluorescence spectra changes (shift of the peak wavelength) depending on pH (pKa: 7.2). This dye allowed us to perform dual-emission ratiometric pH_i imaging using an image splitter with a single EMCCD camera. In this report, we detail our pH_i imaging setup and conditions. Furthermore, we found kinetic differences in the pH_i changes induced by HCO_3^- in human and mouse spermatozoa which could suggest that HCO_3^- influx pathways are distinct in human and mouse spermatozoa.

MATERIALS AND METHODS

Materials

Dimethyl sulfoxide (DMSO, cat. D2650), ammonium chloride (NH_4Cl, cat. A9434), nigericin (cat. N7143), progesterone (cat. P8783), and concanavalin A (cat. C2010) were purchased from Sigma–Aldrich. Pluronic F-127 (cat. P6867), SNARF-5F AM (5-(and-6)-carboxylic acid, acetoxymethyl ester) (cat. S23923), and 2′, 7′-Bis-(2-carboxyethyl)-5-(and-6)-carboxyfluorescein, acetoxymethyl ester (BCECF AM) (cat. B1170) were obtained from ThermoFisher Scientific.

Biological Sample Collection

Human Spermatozoa

Human spermatozoa samples were obtained from healthy donors under written informed consent and with the approval of the Bioethics Committee of the Instituto de Biotecnología, Universidad Nacional Autónoma de México (IBt-UNAM). Only ejaculates that fulfilled the World Health Organization guidelines were used in all the experiments (Cao et al., 2010). Motile cells were recovered using the swim-up technique in HTF medium (in mM: 90 NaCl, 4.7 KCl, 1.6 $CaCl_2$, 0.3 KH_2PO_4, 1.2 $MgSO_4$, 2.8 glucose, 0.3 pyruvic acid, 23.8 HEPES, and 21.4 lactic acid, 25 $NaHCO_3$) pH 7.4 (Mata-Martínez et al., 2013). Briefly, 400 μl of liquefied semen was placed in glass test tubes and 1 ml HTF medium was carefully added on the top of the semen without mixing the phases. Samples were incubated for 1 h at 37°C under 5% CO_2. The upper layer (700 μl) with motile spermatozoa was then collected. Cell density was determined using a Makler chamber and adjusted to 10×10^6 spermatozoa/ml.

Mouse Spermatozoa

All experimental protocols were approved by the Bioethics Committee of the IBt-UNAM). Motile spermatozoa were obtained from epididymal cauda of 3-month-old CD-1 mouse by placing incised epididymis in an Eppendorf tube containing 1 ml of in TYH medium (in mM: 119 NaCl, 4.7 KCl, 1.7 $CaCl_2$, 1.2 KH_2PO_4, 1.2 $MgSO_4$, 5.6 dextrose, 0.5 pyruvic acid, and 20 HEPES) pH 7.4. Spermatozoa were allowed to swim-out during 15 min at 37°C. The upper layer (800 μl) with motile spermatozoa was collected and the cell density was adjusted to 10×10^6 spermatozoa/ml using a Makler counting chamber (Irvine Scientific, Santa Ana, CA, United States).

In vitro Fluorescence Spectra of SNARF-5F

Fluorescence spectra of SNARF-5F were determined with a Perkin-Elmer LS 55 (Perkin-Elmer, Waltham, MA, United States) fluorescence spectrometer using the software FL WinLab version 4.00.03 for data acquisition (**Figure 1**). SNARF-5F non-permeable and AM versions were used at 20 μM final

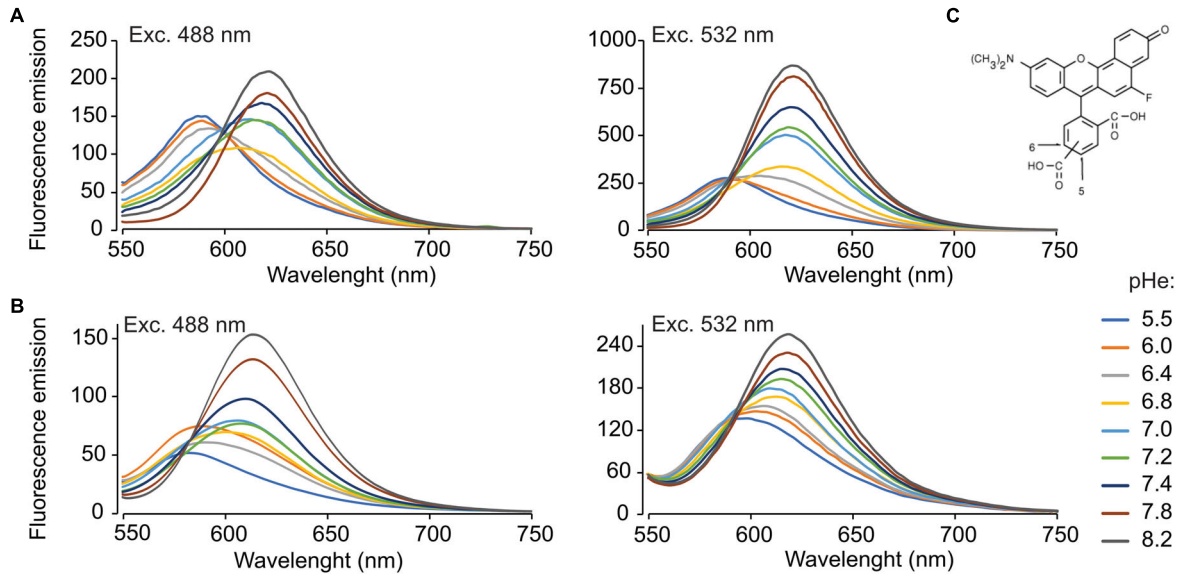

FIGURE 1 | SNARF-5F emission spectra at 488 and 532 nm excitation wavelengths, in 50 mM potassium phosphate buffers at various pH values. Emission spectra of non-permeable SNARF-5F **(A)** using a fixed excitation wavelength of 488 nm (**A**,left) and 532 nm (**A**,right). Emission spectra of SNARF-5F-AM **(B)** with 10×10^6 sperm/ml treated with 0.1% Triton X-100, using a fixed excitation wavelength of 488 nm (**B**,left) and 532 nm (**B**,right). The lines are representative fluorescence spectra at different pH_e (5.5, 6.0, 6.4, 6.8, 7.0, 7.2, 7.4, 7.8, and 8.2), indicated by color lines. **(C)** SNARF-5F chemical structure. Typically, SNARF-5F possess two emission wavelengths, at 575 and 640 nm; $n = 4$.

concentration in 50 mM potassium phosphate buffer (see table in **Supplementary Figure S1**). Multiple spectra were acquired using various excitation wavelengths (405, 440, 465, 488, 510, 532, and 543 nm) and different pH_e (5.5, 6.0, 6.4, 6.8, 7.0, 7.2, 7.4, 7.8, and 8.2) (**Supplementary Figure S1**).

SNARF-5F and BCECF Incorporation Into Spermatozoa

Motile mouse/human spermatozoa (10×10^6/ml) were incubated with 20 μM SNARF-5F AM in the presence of 0.1% pluronic F-127 during 90 min at 37°C with 5% CO_2 in the dark. The cells were washed once by centrifugation at $200 \times g$ for 5 min and resuspended with fresh medium. To obtain fluorescence spectra of SNARF-5F incorporated into spermatozoa, human spermatozoa loaded with SNARF-5F AM were diluted in the media of different pH_e as described above and treated with 0.1% Triton-X 100 detergent. Fluorescence spectra of the lysed spermatozoa were acquired at excitation wavelengths 488 and 532 nm. For single cell recordings, spermatozoa were attached to Concanavalin A-treated coverslips for 2–3 min and mounted in recording chambers.

For BCECF experiments, motile mouse/human spermatozoa (10×10^6/ml) were incubated with 1 μM BCECF AM without pluronic acid during 15 min at 37°C with 5% CO_2 in the dark and the unincorporated dye was removed by centrifugation as the case of SNARF-5F.

Imaging Setup

Single cell images were acquired using two different setups: (1) Olympus iX71 LED-light source epifluorescence microscope and (2) Olympus iX81 laser widefield/total internal reflection fluorescence (TIRF) microscope (Olympus, Japan). The LED setup was equipped with a PlanApo N 60X/1.42 oil objective and a 3A 532 nm LED coupled to Opto-LED light controller (Cairn Research, United Kingdom). The laser setup was equipped with an Apo N (TIRF) 60X/1.49 oil objective and a 488 nm laser with high speed imaging shutter. To acquire dual emission images of SNARF-5F, an image splitter OptoSplit II (Cairn Research, United Kingdom) was used for both setups, LED (with band-pass filter ET 530/30X) and laser. To acquire the images with SNARF-5F, a wide band-pass filter ET 575/50 M (channel 1) and a band-pass filter ET 640/20 M (channel 2) were employed as dual emission filters combined with a dichroic mirror DC 610lp (Chroma Technology, United States) (**Figure 2**). For BCECF experiments, a 3.15 A 465 nm LED (Luminus Devices, Woburn, MA, United States) with bandpass filter HQ 480/40X was used for excitation light, combined with a dichroic mirror (Q505lp) and an emission filter (HQ 535/50M) (Chroma Technology, United States). Each setup has a 512×512 Andor iXon 3 EMCCD camera (model X3 DU897E-CS0) (Oxford Instruments, United Kingdom).

Images were acquired with the software Andor iQ version 2.9.1 (LED set-up) (Oxford Instruments, United Kingdom) and Xcellence version 1.2 (laser set-up) (Olympus, Japan). Fluorescence images of both SNARF-5F and BCECF were taken with 1×1 binning, 5 images/s (5 ips), with an exposure time of 10 ms for the LED setup and 30 ms (laser potency 35%) for the laser setup. Images were analyzed with ImageJ version 1.52n (NIH, United States), obtaining mean fluorescence intensities, selecting heads and flagellum as regions of interest.

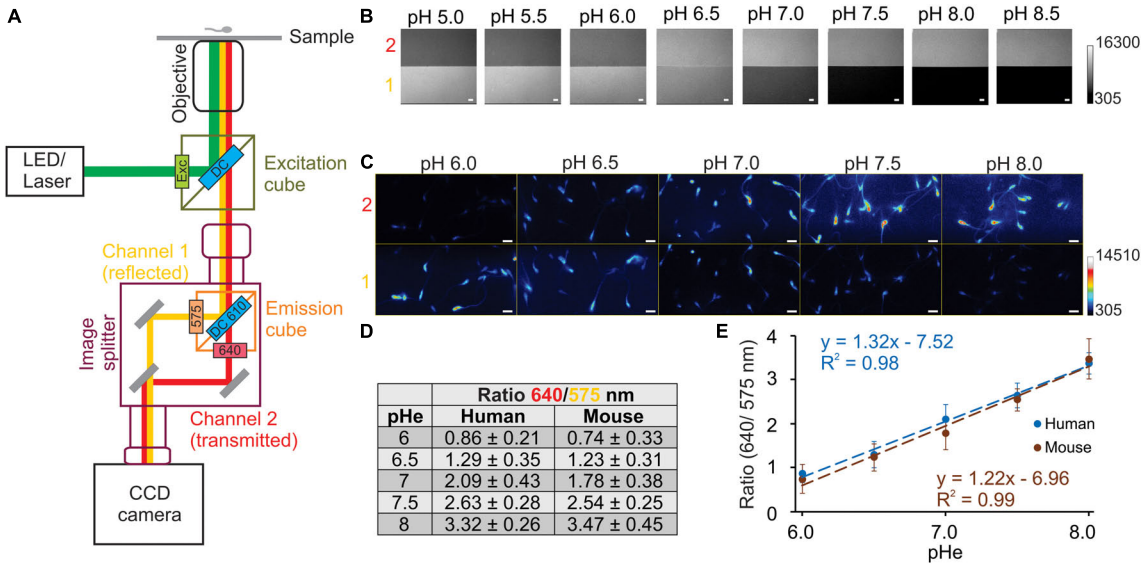

	Ratio 640/575 nm	
pHe	Human	Mouse
6	0.86 ± 0.21	0.74 ± 0.33
6.5	1.29 ± 0.35	1.23 ± 0.31
7	2.09 ± 0.43	1.78 ± 0.38
7.5	2.63 ± 0.28	2.54 ± 0.25
8	3.32 ± 0.26	3.47 ± 0.45

FIGURE 2 | Imaging set-up configuration to visualize the dual emission wavelengths of SNARF-5F. Diagram of imaging set-up **(A)**, indicating LED (532 nm) or laser (488 nm) as an illumination source. A different excitation cube (green square) was used for the LED set-up (ET 530/30X, dichroic mirror DC 550 LP) and the laser set-up (D485/25X, dichroic DC510 LP). To visualize at the same time the two emission wavelengths of SNARF-5F, we used an image splitter (in purple), which has an emission cube (orange square) (ET575/50M, ET640/20M, and dichroic mirror DC610 LP), that divides the emission in reflected (channel 1, corresponding to emission wavelength 575 nm) or transmitted (channel 2, corresponding to emission wavelength 640 nm) images. The image splitter is coupled to the microscope on one side, and to the detector (CCD camera) on the other. Fluorescence images obtained from epifluorescence (laser set-up) microscope with 60× (Plan Apo N, 1.49 numerical aperture) objective, using 20 μM non-permeable SNARF-5F **(B)** or 20 μM SNARF-5F-AM loaded in human and mouse (not shown) spermatozoa in the presence of nigericin 10 μM **(C)** in 50 mM potassium phosphate buffers at indicated pH. **(D)** Ratio values were obtained (referred from panel **C**) at each pH$_e$ (6.0, 6.5, 7.0, 7.5, and 8.0) in human and mouse spermatozoa, using channel 1 (575 nm) and channel 2 (640 nm) fluorescence values. **(E)** Lineal correlation between pH$_e$ and fluorescence ratio in human and mouse spermatozoa, obtaining R^2 = 0.99 and 0.98, respectively. Numbers 1 (yellow) and 2 (red) to the left in panels **B** and **C** refer to channel 1 (emission 575 nm) and channel 2 (emission 640 nm). Scale bar in panels **B** and **C** is equal to 10 μm; n = 3.

In vivo pH$_i$ Calibration

To convert fluorescence data to pH values *in vitro*, the following equation is commonly used:

$$\mathrm{pH} = \mathrm{pK_a} - \log\left[\frac{R - R_B}{R_A - R} \times \frac{F_{B(\lambda_2)}}{F_{A(\lambda_2)}}\right]$$

where R is the ratio $F\lambda_1/F\lambda_2$ of fluorescence intensities (F) measured at two wavelengths λ_1 and λ_2 and the subscripts A and B represent the values at the acidic and basic conditions, respectively (Whitaker et al., 1991). However, it is difficult to maintain live spermatozoa in highly acidic and alkaline condition to obtain $F_{B(\lambda_2)}/F_{A(\lambda_2)}$ values from the same cells. Therefore, we performed *in vivo* pH$_i$ calibration by fixing external pH (pH$_e$) between 6.0 and 8.0 as reported previously (Grillo-Hill et al., 2014). Briefly, spermatozoa suspensions were incubated for 15 min with calibration medium (in mM: 120 KCl, 25 HEPES, 1 $MgCl_2$, and 0.01 nigericin, at different pH$_e$: 6.0, 6.5, 7.0, 7.5, and 8.0, adjusted with KOH). We measured the fluorescence intensity at two emissions, 575 (channel 1) and 640 nm (channel 2), always subtracting the fluorescence background value in each channel. As fluorescence ratio values ($R_{F640/F575}$) have a lineal relation with pH$_i$ values (between 6.0 and 8.0) (**Figures 2D,E**), we used the following equations to estimate pH$_i$ from the fluorescence ratio values, for human: pH$_i$ = ($R_{F640/F575}$ + 6.96)/1.22 and for mouse: pH$_i$ = ($R_{F640/F575}$ + 7.52)/1.32.

Statistical Analysis

The results are expressed as the mean ± SEM of at least three independent experiments (three different donors or mice), with a minimum of 200 cells per condition. The data were analyzed by a comparison test between the groups, using the non-parametric Mann–Whitney U-test with 95% statistical significance. The paired tests were carried out comparing the head and the flagellum of the same cell. Additionally, the Bonferroni correction was used when multiple comparisons were made.

RESULTS

Emission Spectra of SNARF-5F With Distinct Excitation Wavelengths

To perform ratiometric fluorescence measurements with a good signal to noise ratio (S/N ratio), it is important to acquire bright fluorescence images in both channels. In other words, if we detect dim fluorescence signals in one channel, the S/N ratio of the dual-emission ratio values become undesirably low even when we detect bright signals in the other channel. As spermatozoa possess a quite reduced cytoplasm, it is crucial to use an appropriate excitation wavelength and emission filters. Therefore, we first determined the fluorescence spectra of SNARF-5F at several pH$_e$ values (5.5–8.2), exciting with various wavelengths (405–543 nm). As shown in **Supplementary Figure S1**, the

longer excitation wavelength (longer than 465 nm) gives the higher fluorescence intensities in all emission wavelengths we explored (550–750 nm). Namely, 543 nm produced the highest fluorescence values.

Figure 1 illustrates the fluorescence spectra of SNARF-5F at different pH$_e$ (5.5–8.2) excited at 488 and 532 nm. At both exciting wavelengths, the fluorescence intensities around 575 nm (the first peak) decrease when the pH increases, while those of around 640 nm (the second peak) increase at the same conditions. When exciting at 532 nm, the relative fluorescence intensities within the first peak at different pH$_e$ are much smaller than those within the second peak, as reported in the original article of SNARF-5F (Liu et al., 2001). Conversely, the relative fluorescence intensities within the two peaks became almost equal when 488 nm was used as excitation light (**Figure 1A**). In spite of this favorable feature, their absolute fluorescence intensities are small. Considering these characteristics, we selected 532 nm as the best compromise between brightness and peak balance for this study.

To evaluate the incorporation of the membrane permeant dye SNARF-5F AM into the spermatozoa, we incubated human spermatozoa with 20 μM of this dye for 90 min. After the excess dye was washed out by centrifugation, the cells were lysed with 0.1% Triton X-100 and the fluorescence spectra were acquired (**Figure 1B**). The spectra of the dye incorporated into human spermatozoa were not identical to SNARF-5F *in vitro*, suggesting that SNARF-5F AM was not completely hydrolyzed in the cell and/or some of the dye was bound to certain molecules of the cell. Nevertheless, SNARF-5F AM incorporated into the cell responded to pH$_e$ changes similarly to SNARF-5F AM.

Dual-Emission pH$_i$ Imaging System and *in vivo* Calibration of pH$_i$

A conventional dual-emission fluorescence imaging setup usually is composed of an epi-fluorescence microscope, a CCD camera, and a filter wheel, which exchanges two emission filters alternatively. In this type of setup, there is always a time lag between the image in one channel and the image in the other channel. Since spermatozoa are small and motile cells, the presence of a time lag between two images of each channel is undesirable. Therefore, we used an image splitter (Kinosita et al., 1991) that allows the simultaneous capture of the images from the two channels with a single camera (**Figure 2A**). In a common configuration of dual-emission ratiometric imaging, emission lights are divided into two components (two channels) at the isosbestic point, around 595 nm in the case of SNARF-5F AM excited by 532 nm. However, because the fluorescence intensity of the first peak (575 nm) is lower than the second peak (640 nm) as described previously (**Figure 1**), we separated the emission light at 610 nm (about 15 nm longer than the isosbestic point) by a dichroic mirror. Consequently, we collected a wide range of wavelengths, 550–600 nm, as the fluorescence signals in the first channel (channel 1). Then, we collected 630–650 nm wavelengths as the longer wavelength fluorescence (channel 2). This configuration gives us comparable fluorescence intensities from the two channels without the insertion of a neutral density filter (**Figure 2A**).

Figure 2B shows fluorescence images (gray scale) of SNARF-5F in media at different pHs, clearly demonstrating the opposite changes of fluorescence intensity between Channel 1 and Channel 2. Since fluorescence spectra of SNARF-5F and SNARF-5F AM incorporated into human spermatozoa show a slight difference (**Figures 1A,B**), we performed *in vivo* calibration using human spermatozoa to convert the ratio fluorescence values into pH$_i$ values. To perform *in vivo* calibration, spermatozoa pH$_i$ was equilibrated to the pH$_e$ using high K^+ (120 mM) media in the presence of 10 μM nigericin (an ionophore that facilitates K^+/H^+ exchange across the lipid bilayer). **Figure 2C** shows fluorescence images (pseudo color) of human spermatozoa, whose pH$_i$ was fixed at different pH$_e$ (6.0–8.0).

The mean ratio values of fluorescence intensities of the two channels (F640/F575) in distinct pH$_i$ are summarized in **Figure 3C** and these ratio values are plotted as a function of pH$_i$ (**Figure 2D**). The ratio values increase proportionally to pH$_i$ between 6.0 and 8.0 with excellent linearity (human spermatozoa: $R_{F640/F575} = 1.22 \times \mathrm{pH}_i - 6.96$, $R^2 = 0.99$; mouse spermatozoa: $R_{F640/F575} = 1.32 \times \mathrm{pH}_i - 7.52$, $R^2 = 0.98$) (**Figure 2E**).

Phototoxicity of SNARF-5F to Spermatozoa

BCECF is known to be quite phototoxic to spermatozoa and this effect can be easily detected as flagellar beat attenuation and as a decrease in the fluorescence intensity (photo-bleaching) during the intense exposure of excitation light (Nishigaki et al., 2006; González-Cota et al., 2015). In this study, we confirmed the phototoxic effect of BCECF on sperm using the same setup utilized for SNARF-5F (**Supplementary Figure S2**). Particularly, the 488 nm laser excitation attenuated the flagellar beat of human and mouse spermatozoa after around 60 and 20 s illuminations, respectively. Subsequently, notable photobleaching of BCECF was observed in both human and mouse spermatozoa (**Supplementary Figures S2A,C**). On the other hand, LED illumination caused less photobleaching in human spermatozoa (**Supplementary Figure S2B**), but certain level of photobleaching was still observed in 40% of mouse spermatozoa (**Supplementary Figure S2D**). This result suggests that mouse sperm are more susceptible to oxidative stress than human spermatozoa.

In contrast, SNARF-5F incorporated into spermatozoa is much less toxic to the cells than BCECF (**Figure 3**). The fluorescence intensities excited by LED and 488 nm laser (epi-fluorescence mode) did not cause photo-bleaching of the dye during our experimental periods (5 ips for 250 s) (**Figures 3A,B**). However, we observed a slight photobleaching of SNARF-5F when excited by the 488 nm laser in the TIRF configuration (**Figure 3C**). This photobleaching was negligible when we reduced the frequency of image acquisition from 5 to 2.5 ips (data not shown).

Comparison of Epi-Fluorescence and TIRF Images

In our previous study of pH$_i$ imaging (epi-fluorescence mode) of sea urchin spermatozoa using BCECF, fluorescence intensities of

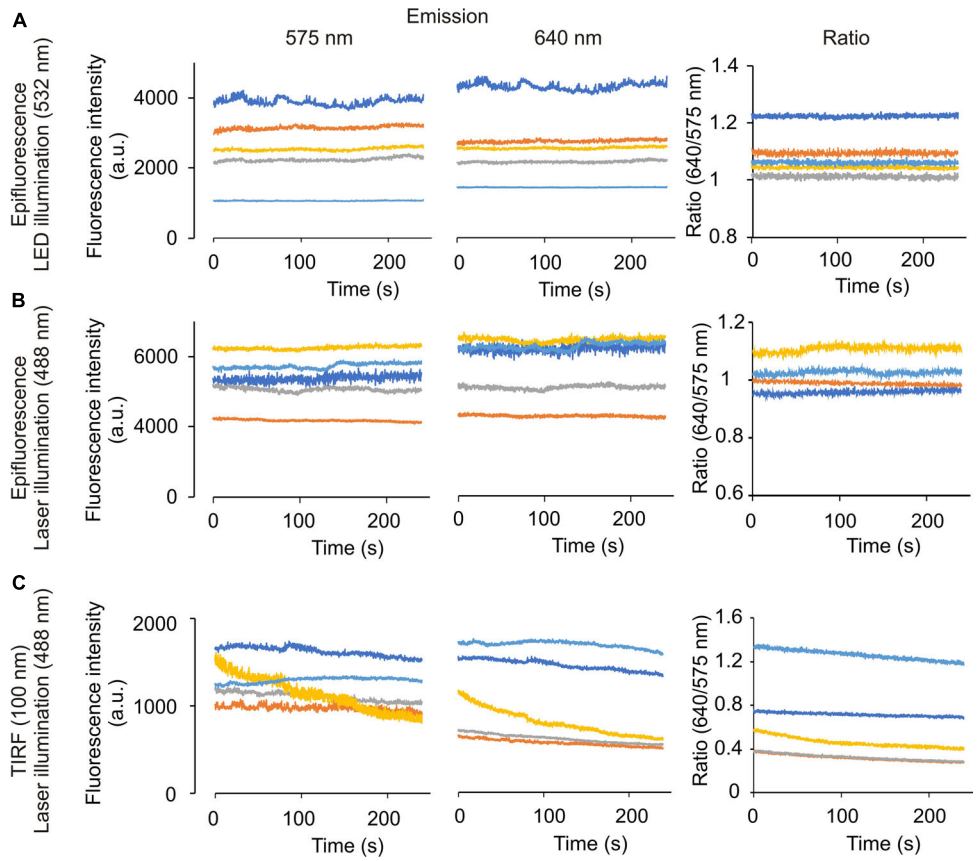

FIGURE 3 | Time-lapse experiments in the microscope set-up did not cause significant photobleaching in mammal spermatozoa, using LED or laser as an illumination source. Representative recordings from emission wavelength time lapse experiments, using 20 μM SNARF-5F-AM in human spermatozoa. Images were taken every 200 ms, exposure time 4 ms with 60× objective. An image splitter was used for the experiments, allowing us to measure emission fluorescence at 575 (left) and 640 (center) nm, and obtaining the ratio from both wavelengths (right). The illumination source was LED 532 **(A)** or laser 488 nm **(B,C)**, in the epifluorescence **(A,B)** or TIRF 100 nm **(C)** configuration. Traces in each panel show representative single cell pH$_i$. Same color at both emission wavelengths indicates the same cell; $n = 3$.

the flagellum were much lower than those of the heads and their fluorescence signals were noisy with a poor S/N ratio (González-Cota et al., 2015). We thought that the use of TIRF would improve this aspect, avoiding the saturation of fluorescence signal in the head. However, the difference of SNARF-5F images between the two configurations (epi-fluorescence and TIRF) was relatively small in both human (**Figure 4A**) and mouse spermatozoa (**Figure 4B**). Particularly, in mouse spermatozoa, the TIRF fluorescence signals in the head and the flagellum (primarily mid piece) are very similar to the epi-fluorescence images. This result is probably due to the thin hook-like shape of the mouse sperm head. As a consequence, an important difference between the two systems (epi-fluorescence and TIRF) is not significant for mouse spermatozoa.

Spermatozoa Responses to pH$_i$ Manipulation

Using the epi-fluorescence configuration with the LED as a light source, we acquired fluorescence images upon pH$_i$ manipulations. During image acquisition, we added HTF or TYH medium as control in human and mouse spermatozoa, respectively. As additional control, 10 mM NH_4Cl and 5 mM HCl were added to increase and reduce the pH$_i$, respectively. The upper panels of **Figures 5A,B** show human sperm fluorescence signals from the two channels in the head and the flagellum, respectively. Changes of fluorescence intensities were observed during the additions even in control conditions (indicated with arrows). Also, fluorescence signals from some cells are noisy probably due to the continuous movement associated to the flagellar beat. Once the dual emission signals were converted into the ratio and pH$_i$ values (**Figures 5A,B**, lower panels), the problems of addition artifacts and movement were eliminated in the both regions, demonstrating the advantage of the dual-emission ratiometric imaging. Additionally, the effects of NH_4Cl and HCl can be clearly observed as an increase and a decrease of the ratio and the pH$_i$, respectively. **Figure 6** basically demonstrates the same results as **Figure 5** but using mouse spermatozoa. In this experiment, the fluorescence signal of the flagellum arises mainly from the mid piece since mouse spermatozoa flagellum is much longer than that of human spermatozoa and therefore it is difficult to capture the

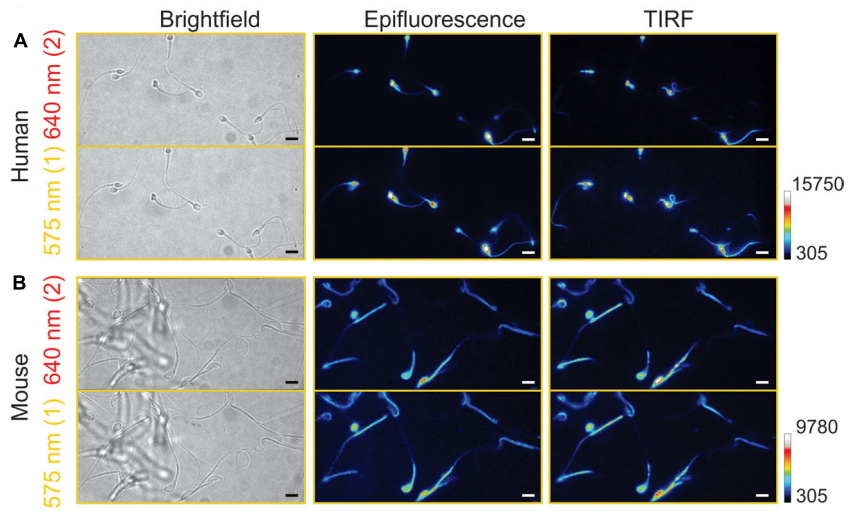

FIGURE 4 | Comparison between epifluorescence and total internal reflection fluorescence (TIRF) images. Representative images from human **(A)** and mouse **(B)** spermatozoa in the two emission channels for SNARF-5F dye, 640 (red) and 575 nm (yellow). Images were taken using the epifluorescence (center) or TIRF (right) configuration. For reference, brightfield images (left) are shown. Scale bar is equal to 10 μm. Reference bar for fluorescence intensity is also depicted. Scale bar is equal to 10 μm; $n = 3$.

image of the entire flagellum of mouse spermatozoa. In these experiments, the average pH$_i$ of non-capacitated human and mouse spermatozoa was 6.72 ± 0.19 (SEM) and 6.63 ± 0.23 (SEM), respectively; $n = 3$.

Response to HCO_3^-

To obtain new insights of mammalian spermatozoa pH$_i$ regulation, we determined the effect of HCO_3^- (10 and 25 mM) on pH$_i$ in non-capacitated human and mouse spermatozoa using our dual-emission imaging system (**Figure 7**). In these experiments, we confirmed that HCO_3^- increases the pH$_i$ of human (**Figure 7A**) and mouse (**Figure 7B**) spermatozoa, in a concentration-dependent manner. We did not observe statistical differences in the pH$_i$ increase induced by HCO_3^- between human and mouse spermatozoa (**Figure 7C**). However, we found a significant difference in the kinetics of the pH$_i$ increase between the two species. Namely, HCO_3^- rapidly increases the pH$_i$ of mouse spermatozoa, and the time to reach 50% of the maximum pH$_i$ increase (t_{50}) was around 10 s. In contrast, HCO_3^- increases human sperm pH$_i$ gradually with a longer t_{50} (40 s) in our experimental conditions (**Figure 7D**). Moreover, the pH$_i$ increase in human spermatozoa was slightly, but significantly, slower in the flagellum compared to the head with 10 and 25 mM HCO_3^- additions.

Response to Progesterone in Human Spermatozoa

In the literature, there is some controversy about the effect of progesterone on human sperm pH$_i$. A decrease (Garcia and Meizel, 1996; Cross and Razy-Faulkner, 1997), no change (Fraire-Zamora and González-Martínez, 2004) or a slow increase (Hamamah et al., 1996) in pH$_i$ have been reported by different groups in response to this hormone. Therefore, we determined the effect of different progesterone concentrations on pH$_i$ in human spermatozoa. **Figure 8** shows that progesterone at 500 nM (I), 1 μM (II), and 10 μM (III) did not change pH$_i$ neither in the head (**Figure 8A**) nor in the flagellum (**Figure 8B**) of these cells. As a control we tested 1 μM monensin, a Na^+ ionophore that exchanges Na^+/H^+ (Babcock, 1983). As anticipated, this ionophore alkalized pH$_i$ in these cells in both head (**Figure 8A**, IV) and flagellum (**Figure 8B**, IV).

DISCUSSION

Advantages of the New System to Determine Spermatozoa pH$_i$

In this study we established a dual-emission ratiometric imaging system using SNARF-5F AM, which has negligible photo-toxicity compared to BCECF (**Figure 3** and **Supplementary Figure S2**). Our system allows determining mammalian spermatozoa (head and flagellum) pH$_i$ with minimum artifacts associated to cell movements and focus alteration upon addition or exchange of bath solutions (**Figures 5–7**). Commonly, the ratio of dual fluorescence signals utilizes the dye isosbestic point (595 nm in our condition). However, the first peak fluorescence intensity (575 nm) of SNARF-5F excited at 532 nm is much smaller than the second peak (640 nm). Therefore, we divided the fluorescence at 610 nm, 15 nm longer than the isosbestic point, and employed a wide band-pass filter (550–600 nm) for Channel 1. In this configuration, fluorescence signals of the two channels are comparable (**Figure 2**), which is a critical point to obtain the ratio values with a good S/N ratio. This type of optical filter configuration (division of fluorescence signals not at the isosbestic point) could be applied to other dual-emission indicators such as GEM-GECO (Zhao et al., 2011) and Asante

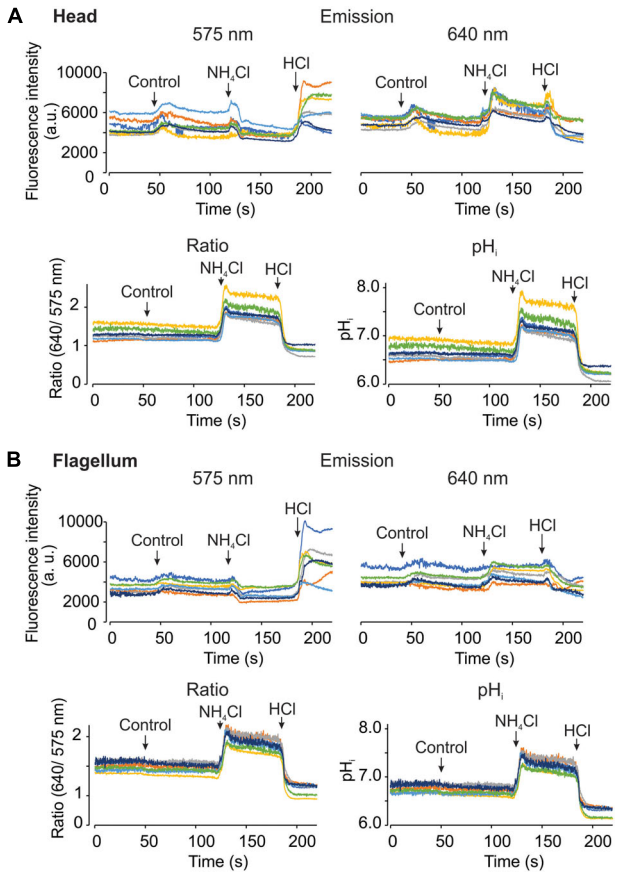

FIGURE 5 | It is possible to measure pH$_i$ using SNARF-5F in human spermatozoa, in the head and flagellum regions. Representative recordings from head **(A)** and flagellum **(B)** regions, measuring fluorescence changes at the two emission wavelengths of SNARF-5F, 575 (Top left) and 640 nm (Top right). Ratio recordings (Bottom left) are obtained from both emission fluorescence values, and converted to pHi (Bottom right) utilizing the calibration curve as shown in **Figure 2**. The micropipette manual addition of HTF medium (control), 10 mM NH_4Cl, and 5 mM HCl is indicated by arrows in each panel. Traces in each panel show representative single cell pH$_i$ responses. Same color at both emission wavelengths and in both regions (head and flagellum) correspond to the same cell; $n = 3$.

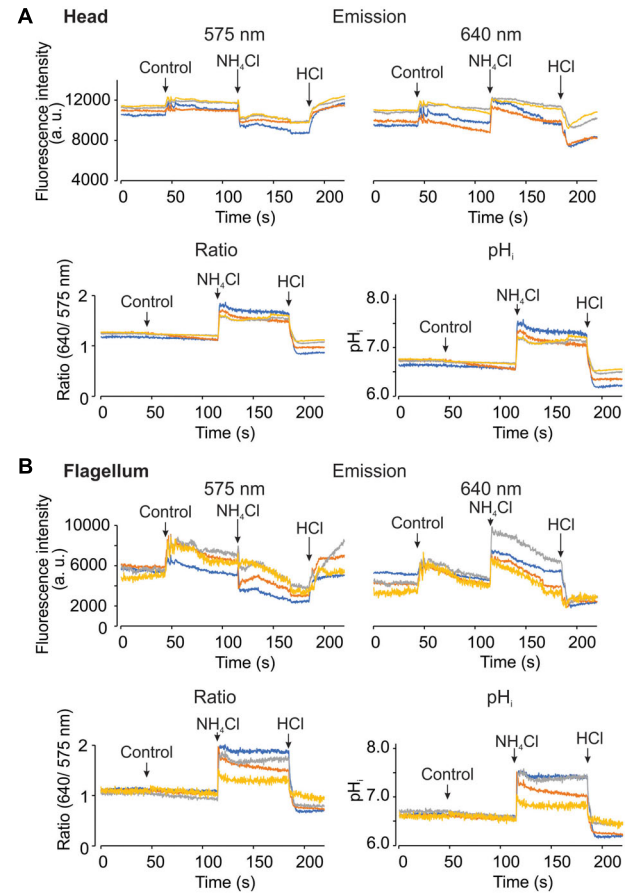

FIGURE 6 | It is possible to measure pH$_i$ using SNARF-5F in mouse spermatozoa, in the head and flagellum regions. Representative fluorescence recordings from head **(A)** and flagellum **(B)** regions, measuring changes at the dual emission wavelengths of SNARF-5F, 575 (Top left) and 640 nm (Top right). Ratio recordings (Bottom left) are obtained from both emission fluorescence values, and converted to pH$_i$ (Bottom right) using the calibration curve shown before. The micropipette manual addition of TYH medium (control), 10 mM NH_4Cl, and 5 mM HCl are indicated by arrows in each panel. Traces in each panel show representative single cell pH$_i$. The same color at both emission wavelengths and in both regions (head and flagellum) correspond to the same cell; $n = 3$.

Calcium Red (Hyrc et al., 2013) because their dual-emission signals are quite asymmetric.

pH$_i$ Calibration

We observed a slight difference between the fluorescence spectra of SNARF-5F *in vitro* and inside human spermatozoa. Therefore, in order to convert the fluorescence emission values into the pH$_i$, we performed an *in vivo* pH$_i$ calibration with human and mouse spermatozoa using a high K^+ solution combined with nigericin in order to equal pH$_i$ to the pH$_e$. This protocol is based on the assumption that the cytoplasmic K^+ concentration is 120 mM in human and mouse spermatozoa, as determined in bovine spermatozoa (Babcock, 1983). Therefore, depending on the real cytoplasmic K^+ concentration in human and mouse spermatozoa, the absolute pH$_i$ values could be different. In our conditions, we determined that the pH$_i$ value in non-capacitated human and mouse spermatozoa is 6.72 ± 0.19 and 6.63 ± 0.23, respectively. These values were measured in the head, but no significant differences were observed in the flagellum (see below). There are several reports of pH$_i$ determinations (most of them in cell population experiments and a few using single cell determination) of non-capacitated spermatozoa from distinct mammalian species: 6.24 (Parrish et al., 1989a) and 6.7 (Vredenburgh-Wilberg and Parrish, 1995) in bovine spermatozoa, 6.55 (Balderas et al., 2013), 6.54 (Zeng et al., 1996), and 6.8 (Carlson et al., 2007) in mouse sperm, and 6.7 (Hamamah et al., 1996; Fraire-Zamora and González-Martínez, 2004) and 6.94 (Cross and Razy-Faulkner, 1997) in human spermatozoa. Our findings that pH$_i$ values of non-capacitated mammalian spermatozoa are >6.5 are consistent with the

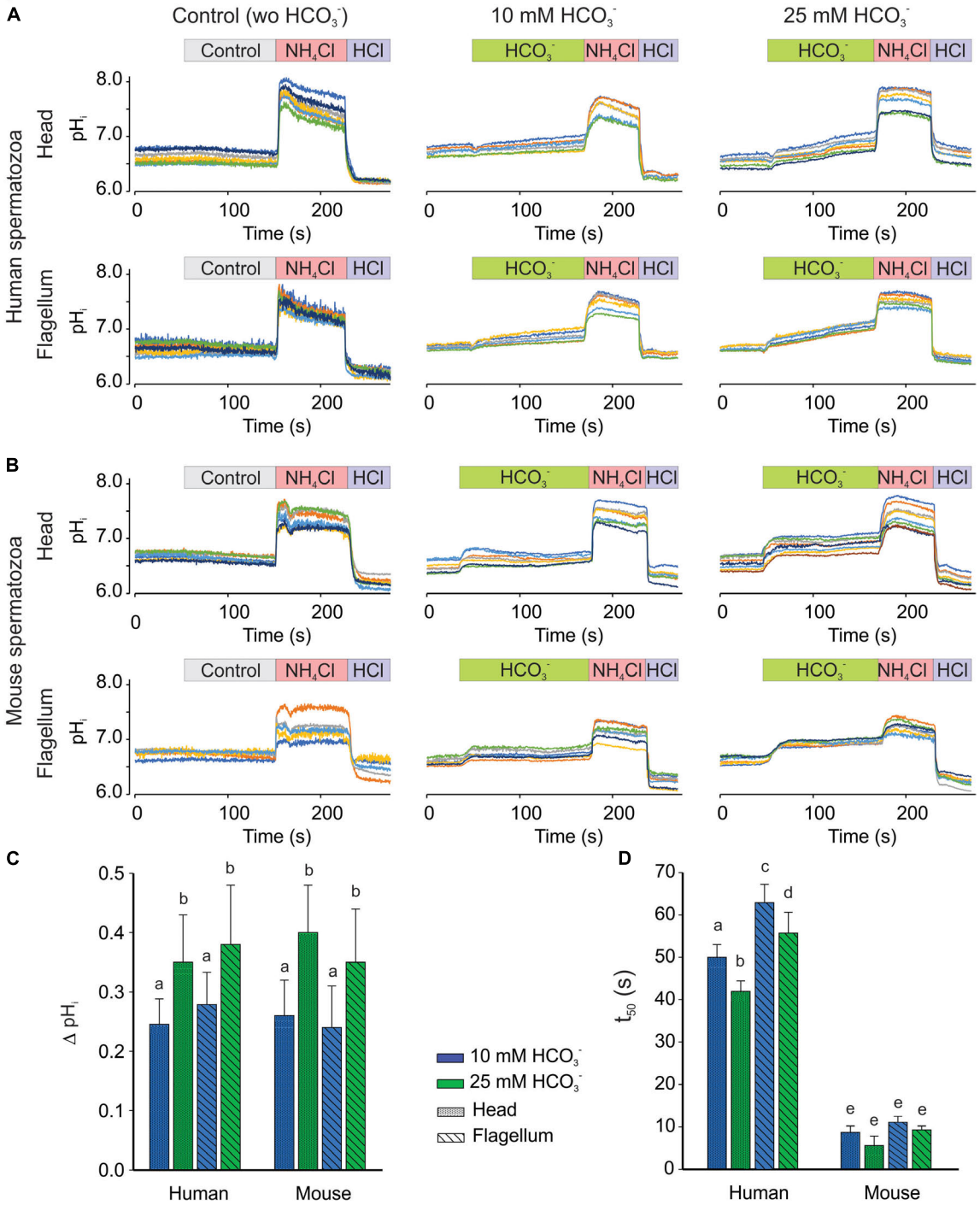

FIGURE 7 | HCO_3^- increased pH$_i$ in a concentration-dependent manner in both, head and flagellum, regions using human and mouse spermatozoa. Representative recordings from human **(A)** and mouse **(B)** spermatozoa, measuring pH$_i$ using 20 μM SNARF-5F in head (Top) and flagellum (Bottom) regions. The perfused addition of medium (HTF and TYH for human and mouse, respectively) (left, control in gray rectangle), 10 (center in green rectangle) or 25 mM (right in green rectangle) HCO_3^- are showed. As positive controls, perfused addition of 10 mM NH_4Cl (red rectangle) and 5 mM HCl (purple rectangle) are showed in each panel. Traces in each panel show representative single cell pH$_i$. Same color in both, head and flagellum, indicate to the same cell. Maximum change in pH$_i$ (ΔpH$_i$) **(C)** and average of t_{50} **(D)**, time to reach 50% of the maximum fluorescent intensity, before and after 10 (blue bars), 25 (green bars) mM HCO_3^- addition, in head (shaded) or flagellum (diagonal lines) regions. The bars in **C,D** indicated means ± SEM. Different letters indicate significant differences at the $p \leq 0.05$ level, according to Mann–Whitney *U*-test; $n = 5$.

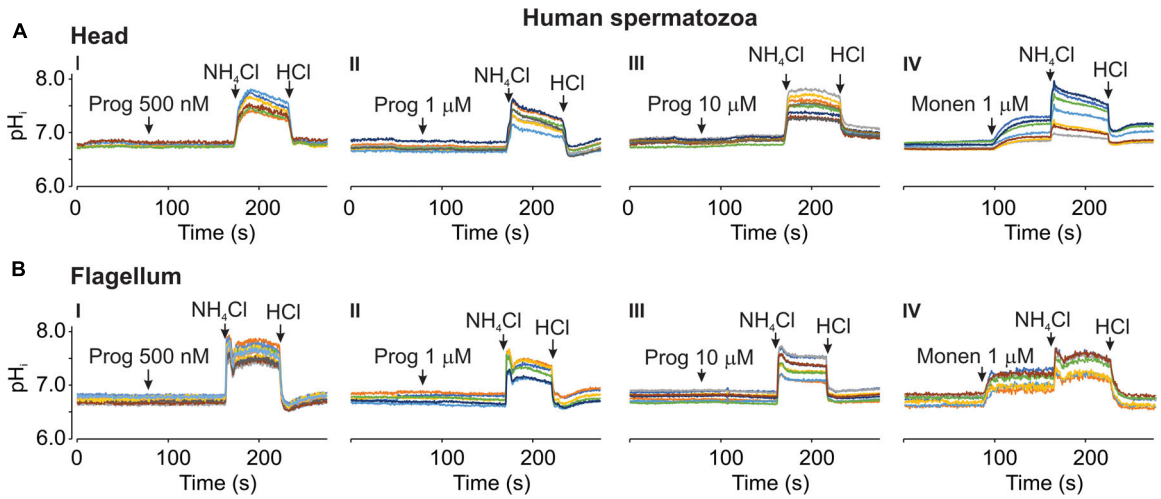

FIGURE 8 | Progesterone did not changed pH$_i$ in human spermatozoa. Representative recordings using 20 μM SNARF-5F in human spermatozoa in the head **(A)** and flagellum **(B)** regions. Micropipette manual progesterone (Prog) additions of 500 nM (I), 1 μM (II), and 10 μM (III), as well as 1 μM of monensin (Monen) (IV) are indicated by arrows in each panel. As controls, 10 mM NH_4Cl and 5 mM HCl additions were performed (see arrows). Traces in each panel show representative single cell pH$_i$. The same color at both emission wavelengths and in both regions (head and flagellum) corresponds to the same cell; $n = 3$.

report that detergent-demembranated bovine spermatozoa do not exhibit motility at pH 6.5, although they are highly motile at pH 7.0 (Ho et al., 2002).

Regional pH$_i$ Difference in the Head and the Flagellum

We did not observe significant differences between the head and the flagellum in the basal pH$_i$ in non-capacitated spermatozoa, although the head pH$_i$ tends to be slightly higher than the flagellar pH$_i$ both in human (6.72 ± 0.19 and 6.69 ± 0.24, respectively) and mouse spermatozoa (6.63 ± 0.23 and 6.60 ± 0.26, respectively). Our results are similar to those reported in bovine spermatozoa (Vredenburgh-Wilberg and Parrish, 1995). In general, the epifluorescent signal from an indicator incorporated into the sperm head is generally much higher than in the flagellum, independently of the species. Therefore, we examined if TIRF microscopy would reduce the fluorescence difference between the head and the flagellum. However, we did not observe significant differences nor advantages of TIRF microscopy compared to epifluorescence microscopy (**Figure 4**) either in mouse or human spermatozoa for measuring pH$_i$. With these data, we can conclude that epifluorescence microscopy with SNARF-5F AM allows performing reliable single spermatozoa pH$_i$ imaging with a good S/N ratio in both spermatozoa head and flagellum (mid piece of flagellum in the case of mouse).

Difference of pH$_i$ Responses to HCO_3^- Between Human and Mouse Spermatozoa

HCO_3^- is an essential ion for mammalian sperm to acquire the ability to fertilize the oocyte (Lee and Storey, 1986). In fact, the HCO_3^- concentrations in rabbit uterine and tubal fluids are approximately twice as high as in the blood plasma, which results in pH values of 7.4 and 8.1–8.3, respectively (Vishwakarma, 1962). In rhesus monkeys, the pH and HCO_3^- concentration in the oviduct lumen change during the menstrual cycle. Namely, these values are similar to those of the blood plasma during the follicular phase, but they suddenly increase concomitantly with ovulation (Maas et al., 1977). This observation supports the importance of HCO_3^- for fertilization in mammals. The principal role of cytoplasmic HCO_3^- in mammalian spermatozoa is considered to be the activation of the soluble adenylyl cyclase, which increases cAMP (Okamura et al., 1985; Buck et al., 1999; Chen et al., 2000), leading to protein kinase A (PKA) stimulation. The enhanced PKA activity increases flagellar beat frequency (Wennemuth, 2003) and elevates CatSper activity (Carlson et al., 2003; Orta et al., 2018), among many other things.

In this work, we observed that HCO_3^- elevates the pH$_i$ in both human and mouse spermatozoa (**Figure 7D**). In contrast, Carlson et al. (2007) reported that HCO_3^- did not induce a pH$_i$ increase in mouse spermatozoa. Interestingly, we found a difference in the kinetics of HCO_3^--induced pH$_i$ increase between the two species (**Figure 7D**), namely a faster increase in mouse compared to human spermatozoa, but of similar magnitude (**Figure 7C**). So far, several mechanisms have been reported for HCO_3^- influx, such as the NBC (Demarco et al., 2003), Cl^-/HCO_3^- exchangers (Chavez et al., 2012), and the CFTR channel (Hernández-González et al., 2007; Xu et al., 2007). However, the physiological relevance of each transporter is unclear as well as differences between the two species. In addition to HCO_3^- transporters, CO_2 diffusion with subsequent hydration by intracellular CA contributes to an increase in cytoplasmic HCO_3^- concentration (Carlson et al., 2007; Wandernoth et al., 2010; José et al., 2015). Curiously, a general CA inhibitor, ethoxyzolamide, potently affects human but not mouse sperm motility (José et al., 2015), suggesting a difference in the involvement of CAs in the motility of the two species. Another

explanation is that human spermatozoa may have higher pH buffering capacity than mouse spermatozoa. This might be correlated to the time required for capacitation (>6 h in human compared to 1–2 h in mouse spermatozoa). Indeed, the pH_i of mammalian spermatozoa studied so far increases around 0.14–0.4 units during capacitation (Parrish et al., 1989b; Vredenburgh-Wilberg and Parrish, 1995; Hamamah et al., 1996; Zeng et al., 1996; Cross and Razy-Faulkner, 1997; Fraire-Zamora and González-Martínez, 2004; Balderas et al., 2013). A significant part of this pH_i change can be attributed to the HCO_3^- influx into the cell. Therefore, further studies are required for a better understanding of the mechanism of HCO_3^--induced pH_i increase during capacitation. The pH_i imaging system established in this study should contribute to this issue.

Effect of Progesterone in Human Spermatozoa

Progesterone increases $[Ca^{2+}]_i$ in human spermatozoa at concentrations as low as 300 nM, through CatSper activation (Tesarik et al., 1992; Harper et al., 2003; Achikanu et al., 2018). Recently it was described that the progesterone receptor in these cells is a α/β hydrolase domain-containing protein (ABHD2), which depletes the endocannabinoid 2-arachinoylglycerol (2AG) from membrane and removes CatSper inactivation (Miller et al., 2016; Mannowetz et al., 2017). In contrast, there is inconsistency regarding how progesterone affects pH_i. Some groups suggest that this hormone acidifies, others that it alkalizes or does not induce pH_i changes (Garcia and Meizel, 1996; Hamamah et al., 1996; Cross and Razy-Faulkner, 1997; Fraire-Zamora and González-Martínez, 2004). In the present work, progesterone did change pH_i in human spermatozoa even at concentrations as high as 10 μM (**Figure 8**). Our result supports that progesterone activates CatSper in a pH-independent manner, possibly exclusively via ABHD2-2AG.

Progesterone-induced Ca^{2+} influx through CatSper may affect the activity of transporters and enzymes that can affect pH_i such as PMCA (Wennemuth et al., 2003; Okunade et al., 2004) and NOX5 (Baker and Aitken, 2004; Musset et al., 2012). Both PMCA and NOX5 may acidify pH_i when they are activated, namely when the $[Ca^{2+}]_i$ is high. However, the pH_i acidification together with the membrane potential depolarization caused by Ca^{2+} influx through CatSper and electron efflux through NOX5 could activate Hv1 channel (Lishko et al., 2010; Berger et al., 2017) and may rapidly neutralize the acidification (alkalize the pH_i). Depending on the experimental conditions, one activity (acidifying or alkalizing) may exceed the other when progesterone stimulates human CatSper. This may account for part of the discrepancies regarding human sperm pH_i responses to progesterone. Further studies are required to confirm this hypothesis.

DATA AVAILABILITY STATEMENT

All datasets generated for this study are included in the article/**Supplementary Material**.

ETHICS STATEMENT

The studies involving human participants/donors were reviewed and approved by the Bioethics Committee of the Instituto de Biotecnología. The donors provided their written informed consent to participate in this study. The animal study was reviewed and approved by the Bioethics Committee of the Instituto de Biotecnología.

AUTHOR CONTRIBUTIONS

TN conceived the project. JC performed most of the experiments and prepared the figures. All authors proposed the experiments, discussed the results, and wrote, revised, and approved the manuscript.

FUNDING

This work was supported by the PAPIIT DGAPA (Grant Numbers IA200419 to JC, IN200919 to AD, IN202519 to CT, and IN205719 to TN) and CONACyT (Fronteras 71).

ACKNOWLEDGMENTS

We thank Gastón Contreras from the National Laboratory in Advanced Microscopy Facilities, in addition to José L. De la Vega-Beltrán, Yoloxóchitl Sánchez-Guevara, and Paulina Torres for technical assistance. Also, we would like to thank Shirley Ainsworth for library services, and the people of the animal facilities Elizabeth Mata, Graciela Cabeza, and Sergio González. We acknowledge Juan Manuel Hurtado, Roberto Rodríguez, Omar Arriaga, and Arturo Ocádiz for computer services.

SUPPLEMENTARY MATERIAL

The Supplementary Material for this article can be found online at: https://www.frontiersin.org/articles/10.3389/fcell.2019.00366/full#supplementary-material

FIGURE S1 | Spectral characterization of the pH sensitive dye SNARF-5F. Representative emission spectra in 405, 440, 465, 488, 510, 532, and 543 nm excitation wavelengths, in 50 mM potassium phosphate buffers at the proportions indicated in Table 1, obtaining pH_e: 5.5, 6.0, 6.4, 6.8, 7.0, 7.2, 7.4, 7.8, and 8.2. The lines are representative fluorescence spectra at indicated excitation wavelength in each pH_e; $n = 3$.

FIGURE S2 | Single cell pH_i measurements with BCECF using laser of led excitation causes significant photobleaching and a reduced response to alkalization and acidification. Representative normalized recordings using BCECF-loaded spermatozoa in human **(A,B)** and mouse **(C,D)**. Laser **(A,C)** and LED **(B,D)** were used as the excitation light source. Arrows indicate the manual addition of 10 mM NH_4Cl and 5 mM HCl in each panel. Each trace represents the response of a single cell; $n = 3$.

REFERENCES

Achikanu, C., Pendekanti, V., Teague, R., and Publicover, S. (2018). Effects of pH manipulation, CatSper stimulation and Ca2+-store mobilization on [Ca2+]i and behaviour of human sperm. *Hum. Reprod.* 33, 1802–1811. doi: 10.1093/humrep/dey280

Acott, T. S., and Carr, D. W. (1984). Inhibition of bovine spermatozoa by caudal epididymal fluid: ii. interaction of pH and a quiescence factor. *Biol. Reprod.* 30, 926–935. doi: 10.1095/biolreprod30.4.926

Babcock, D. F. (1983). Examination of the intracellular ionic environment and of ionophore action by null point measurements employing the fluorescein chromophore. *J. Biol. Chem.* 258, 6380–6389.

Baker, M. A., and Aitken, R. J. (2004). The importance of redox regulated pathways in sperm cell biology. *Mol. Cell. Endocrinol.* 216, 47–54. doi: 10.1016/j.mce.2003.10.068

Balderas, E., Sánchez-Cárdenas, C., Chávez, J. C., De La Vega Beltrán, J. L., Gómez-Lagunas, F., Treviño, C. L., et al. (2013). The anti-inflammatory drug celecoxib inhibits t-type Ca2+ currents in spermatogenic cells yet it elicits the acrosome reaction in mature sperm. *FEBS Lett.* 587, 2412–2419. doi: 10.1016/j.febslet.2013.05.068

Berger, T. K., Fußhöller, D. M., Goodwin, N., Bönigk, W., Khesroshahi, N. D., Brenker, C., et al. (2017). Posttranslational cleavage of Hv1 in human sperm tunes pH- and voltage-dependent gating. *J. Physiol.* 595, 1533–1546. doi: 10.1113/JP273189

Brown, D., Smith, P. J., and Breton, S. (1997). Role of V-ATPase-rich cells in acidification of the male reproductive tract. *J. Exp. Biol.* 200, 257–262.

Buck, J., Sinclair, M. L., Schapal, L., Cann, M. J., and Levin, L. R. (1999). Cytosolic adenylyl cyclase defines a unique signaling molecule in mammals. *Proc. Natl. Acad. Sci. U.S.A.* 96, 79–84. doi: 10.1073/pnas.96.1.79

Cao, X. W., Lin, K., Li, C. Y., and Yuan, C. W. (2010). *A Review of WHO Laboratory Manual for the Examination and Processing of Human Semen*, 5th Edn, Vol. 17. Geneva: World Health Organization, 287.

Carlson, A. E., Hille, B., and Babcock, D. F. (2007). External Ca2+ acts upstream of adenylyl cyclase SACY in the bicarbonate signaled activation of sperm motility. *Dev. Biol.* 312, 183–192. doi: 10.1016/j.ydbio.2007.09.017

Carlson, A. E., Westenbroek, R. E., Quill, T., Ren, D., Clapham, D. E., Hille, B., et al. (2003). CatSper1 required for evoked Ca2+ entry and control of flagellar function in sperm. *Proc. Natl. Acad. Sci. U.S.A.* 100, 14864–14868. doi: 10.1073/pnas.2536658100

Chávez, J. C., De la Vega-Beltrán, J. L., José, O., Torres, P., Nishigaki, T., Treviño, C. L., et al. (2018). Acrosomal alkalization triggers Ca2+ release and acrosome reaction in mammalian spermatozoa. *J. Cell. Physiol.* 233, 4735–4747. doi: 10.1002/jcp.26262

Chávez, J. C., Ferreira, J. J., Butler, A., De La Vega Beltrán, J. L., Treviño, C. L., Darszon, A., et al. (2014). SLO3 K+ channels control calcium entry through CATSPER channels in sperm. *J. Biol. Chem.* 289, 32266–32275. doi: 10.1074/jbc.M114.607556

Chavez, J. C., Hernandez-Gonzalez, E. O., Wertheimer, E., Visconti, P. E., Darszon, A., and Trevino, C. L. (2012). Participation of the Cl-/HCO3- exchangers SLC26A3 and SLC26A6, the Cl- channel CFTR, and the regulatory factor SLC9A3R1 in mouse sperm capacitation. *Biol. Reprod.* 86, 1–14. doi: 10.1095/biolreprod.111.094037

Chen, Y., Cann, M. J., Litvin, T. N., Iourgenko, V., Sinclair, M. L., Levin, L. R., et al. (2000). Soluble adenylyl cyclase as an evolutionarily conserved bicarbonate sensor. *Science* 289, 625–628. doi: 10.1126/science.289.5479.625

Crhisten, R., Schackmann, R. W., and Shapiro, B. M. (1983). Metabolism of Sea Urchin Sperm Interrelationships between intracellular pH, ATPase activity, and mitochondrial respiration. *J. Biol. Chem.* 258, 5392–5399. doi: 10.1086/281606

Cross, N. L., and Razy-Faulkner, P. (1997). Control of human sperm intracellular pH by cholesterol and its relationship to the response of the acrosome to progesterone. *Biol. Reprod.* 56, 1169–1174. doi: 10.1095/biolreprod56.5.1169

Darszon, A., Wood, C. D., Beltrán, C., Sánchez, D., Rodríguez-Miranda, E., Gorelik, J., et al. (2004). Measuring ion fluxes in sperm. *Methods Cell Biol.* 74, 545–576. doi: 10.1016/s0091-679x(04)74022-4

Demarco, I. A., Espinosa, F., Edwards, J., Sosnik, J., De la Vega-Beltrán, J. L., Hockensmith, J. W., et al. (2003). Involvement of a Na+/HCO3- cotransporter in mouse sperm capacitation. *J. Biol. Chem.* 278, 7001–7009. doi: 10.1074/jbc.M206284200

Espinal-Enríquez, J., Priego-Espinosa, D. A., Darszon, A., Beltrán, C., and Martínez-Mekler, G. (2017). Network model predicts that CatSper is the main Ca2+ channel in the regulation of sea urchin sperm motility. *Sci. Rep.* 7:4236. doi: 10.1038/s41598-017-03857-9

Fraire-Zamora, J. J., and González-Martínez, M. T. (2004). Effect of intracellular pH on depolarization-evoked calcium influx in human sperm. *Am. J. Physiol. Cell Physiol.* 287, C1688–C1696. doi: 10.1152/ajpcell.00141.2004

Garcia, M. A., and Meizel, S. (1996). Importance of sodium ion to the progesterone-initiated acrosome reaction in human sperm. *Mol. Reprod. Dev.* 45, 513–520. doi: 10.1002/(sici)1098-2795(199612)45:4<513::aid-mrd14>3.0.co;2-x

González-Cota, A. L., Silva, P. Â, Carneiro, J., and Darszon, A. (2015). Single cell imaging reveals that the motility regulator speract induces a flagellar alkalinization that precedes and is independent of Ca2+ influx in sea urchin spermatozoa. *FEBS Lett.* 589, 2146–2154. doi: 10.1016/j.febslet.2015.06.024

Grillo-Hill, B. K., Webb, B. A., and Barber, D. L. (2014). Ratiometric imaging of pH probes. *Methods Cell Biol.* 123, 429–448. doi: 10.1016/B978-0-12-420138-5.00023-9

Hamamah, S., Magnoux, E., Royere, D., Barthelemy, C., Dacheux, J. L., and Gatti, J. L. (1996). Internal pH of human spermatozoa: effect of ions, human follicular fluid and progesterone. *Mol. Hum. Reprod.* 2, 219–224.

Hamzeh, H., Alvarez, L., Strünker, T., Kierzek, M., Brenker, C., Deal, P. E., et al. (2019). Kinetic and photonic techniques to study chemotactic signaling in sea urchin sperm. *Methods Cell Biol.* 151, 487–517. doi: 10.1016/bs.mcb.2018.12.001

Harper, C. V., Kirkman-Brown, J. C., Barratt, C. L. R., and Publicover, S. J. (2003). Encoding of progesterone stimulus intensity by intracellular [Ca2+] ([Ca2+]i) in human spermatozoa. *Biochem. J.* 372, 407–417. doi: 10.1042/BJ20021560

Hernández-González, E. O., Treviño, C. L., Castellano, L. E., De La Vega-Beltrán, J. L., Ocampo, A. Y., Wertheimer, E., et al. (2007). Involvement of cystic fibrosis transmembrane conductance regulator in mouse sperm capacitation. *J. Biol. Chem.* 282, 24397–24406. doi: 10.1074/jbc.M701603200

Ho, H.-C., Granish, K. A., and Suarez, S. S. (2002). Hyperactivated motility of bull sperm is triggered at the axoneme by Ca2+ and not cAMP. *Dev. Biol.* 250, 208–217. doi: 10.1006/dbio.2002.0797

Ho, H. C., and Suarez, S. S. (2001). Hyperactivation of mammalian spermatozoa: function and regulation. *Reproduction* 122, 519–526. doi: 10.1530/rep.0.1220519

Hyrc, K. L., Minta, A., Escamilla, P. R., Chan, P. P. L., Meshik, X. A., and Goldberg, M. P. (2013). Synthesis and properties of Asante Calcium Red-A novel family of long excitation wavelength calcium indicators. *Cell Calcium* 54, 320–333. doi: 10.1016/j.ceca.2013.08.001

José, O., Torres-Rodríguez, P., Forero-Quintero, L. S., Chávez, J. C., De La Vega-Beltrán, J. L., Carta, F., et al. (2015). Carbonic anhydrases and their functional differences in human and mouse sperm physiology. *Biochem. Biophys. Res. Commun.* 468, 713–718. doi: 10.1016/j.bbrc.2015.11.021

Kinosita, K., Itoh, H., Ishiwata, S., Hirano, K., Nishizaka, T., and Hayakawa, T. (1991). Dual-view microscopy with a single camera: real-time imaging of molecular orientations and calcium. *J. Cell Biol.* 115, 67–73. doi: 10.1083/jcb.115.1.67

Kirichok, Y., Navarro, B., and Clapham, D. E. (2006). Whole-cell patch-clamp measurements of spermatozoa reveal an alkaline-activated Ca2+ channel. *Nature* 439, 737–740. doi: 10.1038/nature04417

Lee, M. A., and Storey, B. T. (1986). Bicarbonate mouse sperm is essential for fertilization of mouse eggs: mouse sperm require it to undergo the acrosome reaction. *Biol. Reprod.* 56, 349–356. doi: 10.1095/biolreprod34.2.349

Lishko, P. V., Botchkina, I. L., Fedorenko, A., and Kirichok, Y. (2010). Acid extrusion from human spermatozoa is mediated by flagellar voltage-gated proton channel. *Cell* 140, 327–337. doi: 10.1016/j.cell.2009.12.053

Lishko, P. V., Botchkina, I. L., and Kirichok, Y. (2011). Progesterone activates the principal Ca2+ channel of human sperm. *Nature* 471, 387–391. doi: 10.1038/nature09767

Liu, J., Diwu, Z., and Leung, W. Y. (2001). Synthesis and photophysical properties of new fluorinated benzo[c]xanthene dyes as intracellular pH indicators. *Bioorg. Med. Chem. Lett.* 11, 2903–2905. doi: 10.1016/S0960-894X(01)00595-9

Maas, D. H., Storey, B. T., and Mastroianni, L. (1977). Hydrogen ion and carbon dioxide content of the oviductal fluid of the rhesus monkey (*Macaca mulatta*). *Fertil. Steril.* 28, 981–985. doi: 10.1016/S0015-0282(16)42801-3

Mannowetz, N., Miller, M. R., and Lishko, P. V. (2017). Regulation of the sperm calcium channel CatSper by endogenous steroids and plant triterpenoids. *Proc. Natl. Acad. Sci. U.S.A.* 114, 5743–5748. doi: 10.1073/pnas.1700367114

Mata-Martínez, E., José, O., Torres-Rodríguez, P., Solís-López, A., Sánchez-Tusie, A. A., Sánchez-Guevara, Y., et al. (2013). Measuring intracellular Ca^{2+} changes in human sperm using four techniques: conventional fluorometry, stopped flow fluorometry, flow cytometry and single cell imaging. *J. Vis. Exp.* 75:50344. doi: 10.3791/50344

Miller, M. R., Mannowetz, N., Iavarone, A. T., Safavi, R., Gracheva, E. O., Smith, J. F., et al. (2016). Unconventional endocannabinoid signaling governs sperm activation via the sex hormone progesterone. *Science* 352, 555–559. doi: 10.1126/science.aad6887

Musset, B., Clark, R. A., DeCoursey, T. E., Petheo, G. L., Geiszt, M., Chen, Y., et al. (2012). NOX5 in human spermatozoa: expression, function, and regulation. *J. Biol. Chem.* 287, 9376–9388. doi: 10.1074/jbc.M111.314955

Navarro, B., Kirichok, Y., Chung, J. J., and Clapham, D. E. (2008). Ion channels that control fertility in mammalian spermatozoa. *Int. J. Dev. Biol.* 52, 607–613. doi: 10.1387/ijdb.072554bn

Nishigaki, T., José, O., González-Cota, A. L., Romero, F., Treviño, C. L., and Darszon, A. (2014). Intracellular pH in sperm physiology. *Biochem. Biophys. Res. Commun.* 450, 1149–1158. doi: 10.1016/j.bbrc.2014.05.100

Nishigaki, T., Wood, C. D., Shiba, K., Baba, S. A., and Darszon, A. (2006). Stroboscopic illumination usine light-emitting diodes reduces phototoxicity in fluorescence cell imaging. *Biotechniques* 41, 191–197. doi: 10.2144/000112220

Okamura, N., Tajima, Y., Soejima, A., Masuda, H., and Sugita, Y. (1985). Sodium bicarbonate in seminal plasma stimulates the motility of mammalian spermatozoa through direct activation of adenylate cyclase. *J. Biol. Chem.* 260, 9699–9705.

Okunade, G. W., Miller, M. L., Pyne, G. J., Sutliff, R. L., O'Connor, K. T., Neumann, J. C., et al. (2004). Targeted ablation of plasma membrane Ca2+-ATPase (PMCA) 1 and 4 indicates a major housekeeping function for PMCA1 and a critical role in hyperactivated sperm motility and male fertility for PMCA4. *J. Biol. Chem.* 279, 33742–33750. doi: 10.1074/jbc.M404628200

Orta, G., Vega-Beltran, J. L., Hidalgo, D., Santi, C. M., Visconti, P., and Darszon, A. (2018). CatSper channels are regulated by protein kinase A. *J. Biol. Chem.* 293, 16830–16841. doi: 10.1074/jbc.RA117.001566

Parrish, J. J., Susko-Parrish, J. L., and Furst, N. L. (1989a). Capacitation of Bovine Sperm by Heparin: inhibitory Effect of Glucose and Role of Intracellular pH. *Biol. Reprod.* 41, 683–699. doi: 10.1095/biolreprod41.4.683

Parrish, J. J., Susko-Parrish, J. L., Handrow, R. R., Sims, M. M., and First, N. L. (1989b). Capacitation of bovine spermatozoa by oviduct fluid. *Biol. Reprod.* 40, 1020–1025. doi: 10.1095/biolreprod40.5.1020

Ren, D., Navarro, B., Perez, G., Jackson, A. C., Hsu, S., Shi, Q., et al. (2001). A sperm ion channel required for sperm motility and male fertility. *Nature* 413, 603–609. doi: 10.1038/35098027

Rink, T. I., Tsien, R. Y., and Pozzan, T. (1982). Cytoplasmic pH and free Mg2+ in lymphocytes. *J. Cell Biol.* 95, 189–196. doi: 10.1083/jcb.95.1.189

Schackmann, R. W., and Boon Chock, P. (1986). Alteration of intracellular [Ca2+] in sea urchin sperm by the egg peptide speract. Evidence that increased intracellular Ca2+ is coupled to Na+ entry and increased intracellular pH. *J. Biol. Chem.* 261, 8719–8728.

Seifert, R., Flick, M., Bönigk, W., Alvarez, L., Trötschel, C., Poetsch, A., et al. (2015). The CatSper channel controls chemosensation in sea urchin sperm. *EMBO J.* 34, 379–392. doi: 10.15252/embj.201489376

Stauss, C. R., Votta, T. J., and Suarez, S. S. (1995). Sperm motility hyperactivation facilitates penetration of the hamster Zona Pellucida'. *Biol. Reprod.* 53, 1280–1285. doi: 10.1095/biolreprod53.6.1280

Suarez, S. S., and Pacey, A. A. (2006). Sperm transport in the female reproductive tract. *Hum. Reprod. Update* 12, 23–37. doi: 10.1093/humupd/dmi047

Tesarik, J., Mendoza, C., Moos, J., Fénichel, P., and Fehlmann, M. (1992). Progesterone action through aggregation of a receptor on the sperm plasma membrane. *FEBS Lett.* 308, 116–120. doi: 10.1016/0014-5793(92)81256-l

Visconti, P. E., Moore, G. D., Bailey, J. L., Leclerc, P., Connors, S. A., Pan, D., et al. (1995). Capacitation of mouse spermatozoa. II. Protein tyrosine phosphorylation and capacitation are regulated by a cAMP-dependent pathway. *Development* 121, 1139–1150.

Vishwakarma, P. (1962). The pH and bicarbonate-ion content of the oviduct and uterine fluids. *Fertil. Sterl.* 13, 481–485. doi: 10.1016/S0015-0282(16)34633-7

Vredenburgh-Wilberg, W. L., and Parrish, J. J. (1995). Intracellular pH of bovine sperm increases during capacitation. *Mol. Reprod. Dev.* 40, 490–502. doi: 10.1002/mrd.1080400413

Wandernoth, P. M., Raubuch, M., Mannowetz, N., Becker, H. M., Deitmer, J. W., Sly, W. S., et al. (2010). Role of carbonic anhydrase IV in the bicarbonate-mediated activation of murine and human sperm. *PLoS One* 5:e15061. doi: 10.1371/journal.pone.0015061

Wang, D., King, S. M., Quill, T. A., Doolittle, L. K., and Garbers, D. L. (2003). A new sperm-specific Na+/H+ Exchanger required for sperm motility and fertility. *Nat. Cell Biol.* 5, 1117–1122. doi: 10.1038/ncb1072

Wennemuth, G. (2003). Bicarbonate actions on flagellar and Ca2+-channel responses: initial events in sperm activation. *Development* 130, 1317–1326. doi: 10.1242/dev.00353

Wennemuth, G., Babcock, D. F., and Hille, B. (2003). Calcium clearance mechanisms of mouse sperm. *J. Gen. Physiol.* 122, 115–128. doi: 10.1085/jgp.200308839

Whitaker, J. E., Haugland, R. P., and Prendergast, F. G. (1991). Spectral and photophysical studies of benzo[c]xanthene dyes: dual emission pH sensors. *Anal. Biochem.* 194, 330–344. doi: 10.1016/0003-2697(91)90237-N

Windler, F., Bönigk, W., Körschen, H. G., Grahn, E., Strünker, T., Seifert, R., et al. (2018). The solute carrier SLC9C1 is a Na+/H+-exchanger gated by an S4-type voltage-sensor and cyclic-nucleotide binding. *Nat. Commun.* 9:2809. doi: 10.1038/s41467-018-05253-x

Xu, W. M., Shi, Q. X., Chen, W. Y., Zhou, C. X., Ni, Y., Rowlands, D. K., et al. (2007). Cystic fibrosis transmembrane conductance regulator is vital to sperm fertilizing capacity and male fertility. *Proc. Natl. Acad. Sci. U.S.A.* 104, 9816–9821. doi: 10.1073/pnas.0609253104

Zeng, Y., Oberdorf, J. A., and Florman, H. M. (1996). pH regulation in mouse sperm: identification of Na+-, Cl–, and[formula]dependent and arylaminobenzoate-dependent regulatory mechanisms and characterization of their roles in sperm capacitation. *Dev. Biol.* 173, 510–520. doi: 10.1006/dbio.1996.0044

Zhao, Y., Araki, S., Wu, J., Teramoto, T., Chang, Y.-F., Nakano, M., et al. (2011). An expanded palette of genetically encoded Ca2+ indicators. *Science* 333, 1888–1891. doi: 10.1126/science.1208592

Zhou, H. X., and Pang, X. (2018). Electrostatic interactions in protein structure, folding, binding, and condensation. *Chem. Rev.* 118, 1691–1741. doi: 10.1021/acs.chemrev.7b00305

Conflict of Interest: The authors declare that the research was conducted in the absence of any commercial or financial relationships that could be construed as a potential conflict of interest.